Experiments in Fluids 37 (2004) 469–482
DOI 10.1007/s00348-004-0813-3

Measurement of the turbulent kinetic energy budget of a planar wake flow in pressure gradients

Xiaofeng Liu, Flint O. Thomas

Abstract Turbulent kinetic energy (TKE) budget measurements were conducted for a symmetric turbulent planar wake flow subjected to constant zero, favorable, and adverse pressure gradients. The purpose of this study is to clarify the flow physics issues underlying the demonstrated influence of pressure gradient on wake development, and provide experimental support for turbulence modeling. To ensure the reliability of these notoriously difficult measurements, the experimental procedure was carefully designed on the basis of an uncertainty analysis. Three different approaches were applied for the estimate of the dissipation term. An approach for the determination of the pressure diffusion term together with correction of the bias error associated with the dissipation estimate is proposed and validated with the DNS results of Moser et al (J Fluid Mech (1998) 367:255–289). This paper presents the results of the turbulent kinetic energy budget measurement and discusses their implications for the development of strained turbulent wakes.

1 Introduction

The response of a symmetric, turbulent plane near-wake to constant favorable and adverse streamwise pressure gradients was the focus of an experimental investigation reported by Liu et al (2002). Their work was motivated by its relevance to high-lift for commercial transport aircraft. In such applications, the wake from upstream elements in a multi-element airfoil configuration develops in a strong pressure gradient environment. The nature of the wake's response to the imposed pressure field will significantly affect the overall aerodynamic performance of the high-lift system. The results presented by Liu et al demonstrate that the mean flow and turbulence quantities in the wake are extremely sensitive to the applied pressure gradient. For example, even a modest adverse pressure gradient was found to have a profound effect on increasing wake spreading and reducing the maximum velocity defect decay rate. Along with the enhanced wake widening, the adverse pressure gradient condition was found to sustain higher levels of turbulent kinetic energy over larger streamwise distances than in the corresponding zero pressure gradient wake. In contrast, the favorable pressure gradient case exhibited a reduced spreading rate, increased defect decay rate, and a more rapid streamwise decay of turbulent kinetic energy relative to the zero pressure gradient case.

One of the most physically descriptive measures by which the evolution of a turbulent flow may be assessed is the turbulent kinetic energy per unit mass (TKE). Its budget, which examines the balance and contribution of different mechanisms such as convection, production, diffusion and dissipation in the TKE transport equation, provides insight into the physics of the flow and suggests strategies for turbulence modeling. Given the significant effect that the imposed pressure gradient has upon the evolution of the wake turbulence quantities, as demonstrated by Liu et al and Carlson et al (2001), it is of interest to examine in detail the TKE budget for the strained wake. Since direct numerical simulation (DNS) is limited to low turbulent Reynolds numbers, experiment is still the only feasible approach for obtaining the TKE budget in turbulent flows at high Reynolds numbers.

The measurement of the TKE budget in free shear flows has been the focus of several previous studies. These include Wygnanski and Fiedler (1969), Panchapakesan and Lumley (1993), George and Hussein (1991), Hussein et al (1994), Heskestad (1965) and Bradbury (1965) in jet flows, Wygnanski and Fiedler (1970) in a planar mixing layer, Raffoul et al (1995) and Browne et al (1987) in bluff body wakes, Patel and Sarda (1990) in a ship wake, and Faure and Robert (1969) in the wake of a self-propelled body.

A series of turbulent kinetic energy (TKE) budget measurements were conducted for the symmetric, turbulent planar wake flow subjected to constant zero, favorable, and adverse pressure gradients. This paper will focus on the measurement procedure that was developed in order to

Received: 24 November 2003 / Accepted: 9 March 2004
Published online: 6 July 2004

X. Liu, F. O. Thomas (✉)
Center for Flow Physics and Control,
University of Notre Dame, Notre Dame,
Indiana 46556-5684, USA
E-mail: Flint.O.Thomas.1@nd.edu

Present address: X. Liu
Department of Mechanical Engineering,
The Johns Hopkins University, Baltimore,
Maryland 21218, USA

This research was supported by NASA Langley Research Center, Hampton, VA under Grant No. NASA NAG1-1987, monitored by Ben Anders. The authors would also like to thank Michael M. Rogers of the NASA Ames Research Center for providing the DNS results.

measure the strained wake TKE budget. Special consideration is given to the measurement of the dissipation term, and a comparison of three different methods is presented. The results are compared with the DNS wake simulations at lower Reynolds number conducted by Moser et al (1998). To our knowledge, direct comparison of TKE budget measurement with DNS simulation results has not been previously reported in the literature. The resulting wake TKE budgets are presented and their implications for the development of strained turbulent wakes are discussed.

2
Experimental set-up

2.1
Wind tunnel

The experiments were performed in an open-return subsonic wind tunnel facility located at the Center for Flow Physics and Control at the University of Notre Dame. This facility has been documented in detail in Liu (2001) as well as in Figs. 1 and 2 of Liu et al (2002). Therefore, only essential aspects will be described here.

Ambient laboratory air is drawn into a square tunnel inlet contraction of dimension 2.74 m on a side with a contraction ratio of 20:1. Twelve turbulence reduction screens at the tunnel inlet yield a very uniform test section velocity profile, with a free stream fluctuation intensity level that is less than 0.1% (and less than 0.06% for frequencies greater than 10 Hz).

The reported experiments utilize two consecutive test sections. The upstream test section is 1.83 m in length, 0.61 m in width and 0.36 m in height. This section contains a wake-generating plate (described below) while the second forms a diffuser section which is used to produce the desired constant adverse/favorable pressure gradient environment for wake development. The top and bottom walls of the diffuser are made of sheet metal, and their contour is fully adjustable by means of seven groups of turnbuckles in order to create the desired constant streamwise pressure gradient environment.

In this paper x, y, and z denote the streamwise, lateral, and spanwise spatial coordinates, respectively.

2.2
Wake-generating body

The wake-generating body is a Pexiglas plate (aligned with the flow direction) with chord length of 1.22 m and a thickness of 17.5 mm. The plate leading-edge consists of a circular arc with distributed roughness which gives rise to

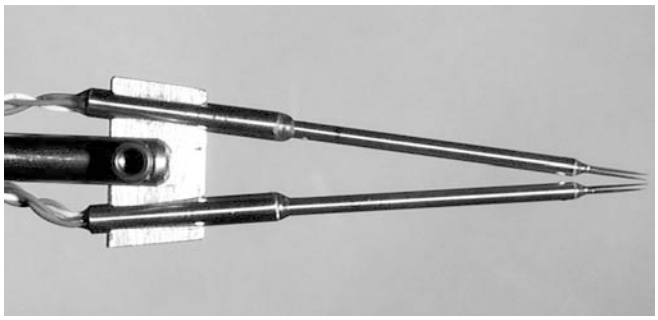

Fig. 2. Twin X-wire probe configuration

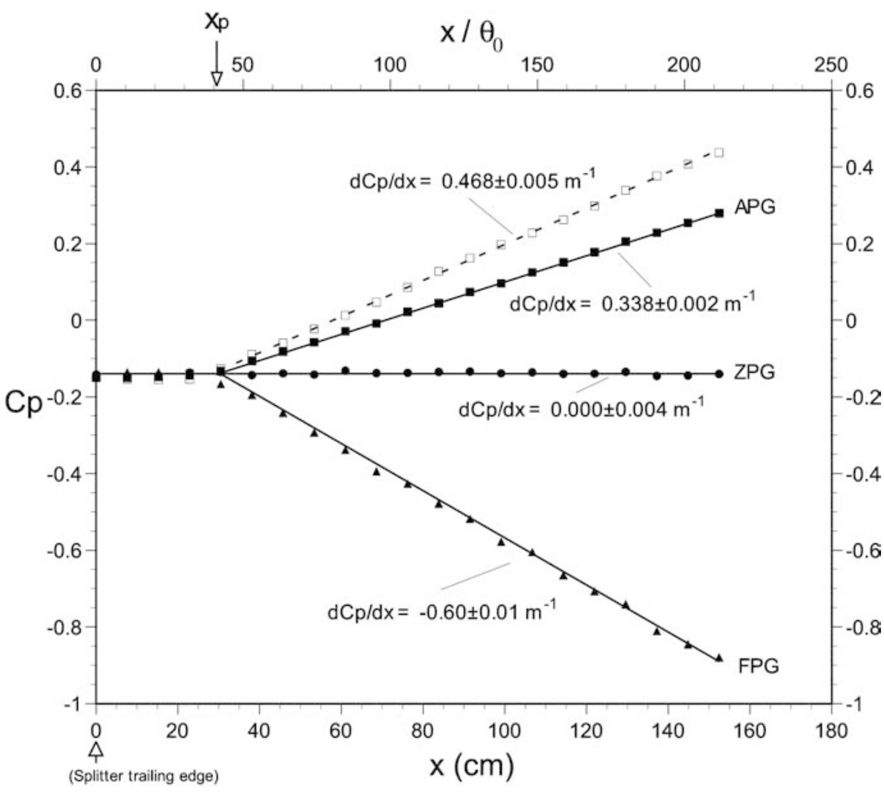

Fig. 1. Experimentally-measured streamwise pressure distributions for zero, adverse and favorable pressure gradient cases

turbulent boundary layers that develop over the top and bottom surfaces of the plate. The last 0.2 m of the plate consists of a 2.2° linear, symmetric taper down to a trailing edge of 1.6 mm thickness. The splitter plate model is sidewall mounted in the test section, with endplates used to minimize the influence of tunnel sidewall boundary layers. The thickness of each endplate is 6 mm, and it spans from the leading edge to the 83% chord location of the wake-generating plate.

2.3
Streamwise pressure gradients

The streamwise pressure gradient is imposed on the wake by means of fully adjustable top and bottom wall contours of the diffuser test section. The flexible walls are iteratively adjusted by means of seven groups of turnbuckles, until the desired constant streamwise pressure gradient dC_p/dx is attained. The streamwise pressure distribution was measured by means of a series of static pressure taps located on one flat sidewall of the diffuser test section at the same lateral (y) location as the centerline of the wake. LDV measurements of the centerspan streamwise distribution of mean velocity, $\bar{U}(x, y=0, z=0)$, were found to be fully consistent with the measured wall pressure variation, thereby confirming the suitability of the pressure tap placement and its use in the characterization of the streamwise pressure gradient imposed on the wake. The imposed pressure will be expressed in terms of a pressure coefficient,$C_p = (P(x)-P_\infty)/q_\infty$, where $P(x)$ is the local static pressure in the diffuser, and P_∞ and q_∞ are the static and dynamic pressures, respectively, upstream of the wake generating plate.

Three sets of experiments were conducted: 1) a zero pressure gradient (ZPG) base flow condition, $dC_p/dx=0.0\ \mathrm{m}^{-1}$; 2) a constant adverse pressure gradient (APG) condition with $dC_p/dx=0.338\ \mathrm{m}^{-1}$, and; 3) a constant favorable pressure gradient (FPG) condition with $dC_p/dx=-0.60\ \mathrm{m}^{-1}$. The zero pressure gradient wake served as an essential baseline case for comparison with the nonzero pressure gradient wake development. In each case, a common zero pressure gradient zone occurs immediately downstream of the splitter plate trailing edge in order to ensure that the wake initial condition is identical. The relative error in the imposed constant pressure gradient is never more than 1.7% to the 95% confidence level.

The measured streamwise pressure distributions corresponding to these different experimental conditions are shown in Fig. 1. As indicated, the pressure gradients are initially applied downstream of the plate trailing edge at a common location designated $x_p \approx 40\ \theta_0$ (where θ_0 is the initial wake momentum thickness). In this manner, the initial conditions at the trailing edge of the plate are identical in each case. Also shown in this figure is a larger adverse pressure gradient case that was run but found to give rise to intermittent, unsteady flow separation near the aft portion of the diffuser wall. For this reason, measurements for this case will not be presented. It may be regarded as an effective upper limit on the magnitude of the constant adverse pressure gradient that can be produced by the diffuser without incurring intermittent, unsteady flow separation effects. The diffuser wall coordinates corresponding to each pressure gradient case shown in Fig. 1 can be found in the Appendix of Liu et al (2002).

The quality of the flow field in the diffuser section was carefully examined. These measurements revealed that the mean flow remains spanwise uniform in the diffuser test section up to the last measurement station at $x=1.52$ m.

2.4
Basic flow parameters

The experiments were performed at a Reynolds number $Re=2.4\times10^6$, based on the chord length of the plate and a free stream velocity of 30.0±0.2 m/s for all pressure gradient cases. The initial wake momentum thickness was$\theta_0=7.2$ mm, corresponding to a Reynolds number based on the initial wake momentum thickness $Re_\theta=1.5\times10^4$. The wind tunnel wall boundary layer thickness (99%U_e) is approximately 19 mm at the streamwise location corresponding to the trailing edge of the splitter plate.

2.5
Flow field diagnostics

A multi-channel TSI IFA-100 constant temperature anemometer was utilized, together with a variety of hot-wire probes, in order to acquire the required time-series velocity fluctuation data. For measurements of the streamwise and lateral or spanwise component velocity, Auspex type AHWX-100 miniature X-wire probes were used. These probes utilize tungsten sensors with a nominal diameter of 5 μm and a sensor length of approximately 1.2 mm. In addition to the X-wire probes, a dual parallel sensor probe (Auspex type AHWG-100) was required for some of the fluctuating derivative measurements in the dissipation estimate. The spacing between the dual sensors of the parallel probe is 0.3 mm, and the sensor length was approximately 0.9 mm. In comparison, the estimated Kolmogorov length scale for the wake flow is approximately 0.1 mm. The effect of the limited spatial resolution of the probes used for fluctuating derivative measurements is discussed in Sect. 4.4.

For the hot-wire measurements, the anemometer output was anti-alias filtered at 20 kHz and digitally sampled at 40 kHz. The 20 kHz Nyquist frequency was chosen to correspond approximately to the highest resolvable frequency of the hot-wire probes at the measurement location for the TKE budget estimate, $x=101.6$ cm ($x/\theta_0=141$). The total record length at each measurement point is 13.1 s, which yielded fully converged turbulence statistics.

In the following section, a dissipation measurement technique based on the assumption of locally axisymmetric, homogeneous turbulence is described. This requires the measurement of the mean-square fluctuating derivative $\overline{\left(\frac{\partial v'}{\partial z}\right)^2}$which cannot be obtained from a single X-wire probe. For this measurement a twin X-wire probe configuration as shown in Fig. 2 was used. The spacing between the centers of the two X-wire probes is approximately 1.3 mm, as determined from an enlarged digital image of the twin X-wire configuration.

3 Turbulent kinetic energy transport equation

A generic form of the turbulent kinetic energy transport equation, valid for incompressible flow (see Hinze 1975) is given by

$$\frac{Dk}{Dt} = -\frac{\partial}{\partial x_i}\overline{u'_i\left(\frac{p'}{\rho}+k'\right)} - \overline{u'_iu'_j}\frac{\partial \overline{U_j}}{\partial x_i} + \nu\frac{\partial}{\partial x_i}\overline{u'_j\left(\frac{\partial u'_i}{\partial x_j}+\frac{\partial u'_j}{\partial x_i}\right)} - \nu\overline{\left(\frac{\partial u'_i}{\partial x_j}+\frac{\partial u'_j}{\partial x_i}\right)\frac{\partial u'_j}{\partial x_i}} \tag{1}$$

where $k = \frac{1}{2}\overline{u'_iu'_i}$ is the mean turbulent kinetic energy per unit mass, and $k' = \frac{1}{2}u'_iu'_i$ is the fluctuating turbulent kinetic energy per unit mass. The left hand side represents the material derivative of turbulent kinetic energy. The terms on the right hand side are, respectively, the effective diffusion of turbulent kinetic energy (by velocity fluctuations and pressure-velocity correlations), turbulence production, reversible viscous work, and turbulence dissipation to heat. Equation 1 may be written in the equivalent form,

$$\frac{Dk}{Dt} = -\frac{\partial}{\partial x_i}\overline{u'_i\left(\frac{p'}{\rho}+k'\right)} - \overline{u'_iu'_j}\frac{\partial \overline{U_j}}{\partial x_i} + \nu\frac{\partial^2 k}{\partial x_i \partial x_i} - \nu\overline{\frac{\partial u'_j}{\partial x_i}\frac{\partial u'_j}{\partial x_i}} \tag{2}$$

It is important to point out that the last term in (2) is not equivalent to the dissipation term in (1). In fact, only if the turbulent flow is homogeneous does the last term on the right hand side of (2) become the proper form for the dissipation. The difference lies in the cross-derivative correlation terms which to-date have not been accurately measured, although there was an attempt to do so by Browne et al (1987). Therefore, as in all other previously-reported efforts to measure the turbulent kinetic energy budget in free shear flows, a concession is made at the outset and utilize Eq. 2 is utilized as the basis for our measurements. The use of the nine-term homogeneous approximation for dissipation is reasonable given the fact that high Reynolds number turbulent flows tend to approach a state of homogeneity at the smallest scales characteristic of the dissipative range.

For the planar turbulent wake under consideration here, we denote the streamwise, lateral and spanwise spatial coordinates as x_1,x_2 and x_3 (which are equivalent to x, y, z), respectively. The corresponding mean velocity components are denoted as $\bar{U}_1$, $\bar{U}_2$, and $\bar{U}_3$(equivalent to U,V, and W) and the fluctuating velocity components as u'_1,u'_2, and u'_3 (equivalent to u, v, and w). For steady, 2-D flow in the mean, we have $\frac{\partial}{\partial t}\overline{()} = 0$, $\overline{U}_3 = 0$ and $\frac{\partial}{\partial x_3}\overline{()} = 0$. Also, from the continuity equation, we have $\frac{\partial \overline{U_2}}{\partial x_2} = -\frac{\partial \overline{U_1}}{\partial x_1}$. Therefore Eq. 2 can be simplified to a form appropriate for the planar turbulent wake flow as follows:

$$\begin{gathered}
0 = -\overline{U_1}\frac{\partial k}{\partial x_1} - \overline{U_2}\frac{\partial k}{\partial x_2} \\
\text{Convection} \\
-\frac{\partial}{\partial x_1}\overline{u'_1\frac{p'}{\rho}} - \frac{\partial}{\partial x_2}\overline{u'_2\frac{p'}{\rho}} \\
\text{Pressure Diffusion} \\
-\frac{\partial}{\partial x_1}\frac{1}{2}\overline{(u'^3_1 + u'_1u'^2_2 + u'_1u'^2_3)} - \frac{\partial}{\partial x_2}\frac{1}{2}\overline{(u'^2_1u'_2 + u'^3_2 + u'_2u'^2_3)} \\
\text{Turbulence Diffusion} \\
-\left(\overline{u'^2_1} - \overline{u'^2_2}\right)\frac{\partial \overline{U_1}}{\partial x_1} - \overline{u'_1u'_2}\left(\frac{\partial \overline{U_1}}{\partial x_2} + \frac{\partial \overline{U_2}}{\partial x_1}\right) \\
\text{Production} \\
+\nu\frac{\partial^2 k}{\partial x_1^2} + \nu\frac{\partial^2 k}{\partial x_2^2} \\
\text{Viscous Diffusion} \\
-\nu\left[\overline{\left(\frac{\partial u'_1}{\partial x_1}\right)^2} + \overline{\left(\frac{\partial u'_1}{\partial x_2}\right)^2} + \overline{\left(\frac{\partial u'_1}{\partial x_3}\right)^2}\right. \\
+\overline{\left(\frac{\partial u'_2}{\partial x_1}\right)^2} + \overline{\left(\frac{\partial u'_2}{\partial x_2}\right)^2} + \overline{\left(\frac{\partial u'_2}{\partial x_3}\right)^2} \\
\left.+\overline{\left(\frac{\partial u'_3}{\partial x_1}\right)^2} + \overline{\left(\frac{\partial u'_3}{\partial x_2}\right)^2} + \overline{\left(\frac{\partial u'_3}{\partial x_3}\right)^2}\right] \\
\text{Dissipation}
\end{gathered} \tag{3}$$

Equation 3 provides the framework to be used for the measurement of the TKE budget in the wake. By measuring the individual terms in Eq. 3, the TKE budget for the turbulent planar wake flow in pressure gradient can be constructed. The approach utilized for the measurement of each term is briefly addressed below.

3.1 Convection term

The convection term consists of two parts, the streamwise convection $-\overline{U_1}\frac{\partial k}{\partial x_1}$ and the lateral convection $-\overline{U_2}\frac{\partial k}{\partial x_2}$. Both can be measured directly. An X-wire probe is used to obtain both $\bar{U}_1$ and $\bar{U}_2$as well as the three normal-component stresses required for calculation of the cross-stream profiles of k. The streamwise spatial derivative $\frac{\partial k}{\partial x_1}$ is obtained from the measurement of k at three adjacent streamwise measurement stations via a finite difference approximation. Details of how streamwise derivatives are computed are discussed in Sect. 3.7 of the paper. The lateral spatial derivative $\frac{\partial k}{\partial x_2}$ is obtained from differentiating an optimum fit to a high spatial resolution lateral profile of k.

3.2 Pressure diffusion term

The pressure diffusion term is not directly measurable. In the jet studies by Wygnanski and Fiedler (1969) and Gutmark and Wygnanski (1976), this term was inferred from a forced balance of the turbulent kinetic energy equation. In a more recent axisymmetric jet study by Panchapakesan and Lumley (1993), the pressure transport term was simply neglected. In the cylinder wake study by Browne et al (1987), it was concluded that the pressure transport term (obtained by forcing a balance of the turbulent kinetic energy equation) was approximately equal to zero. In the jet flow measurement conducted by Hussein et al (1994), they ignored the term $\left(\frac{\overline{u'_1p'}}{\rho}\right)$and attempted to estimate $\overline{\left(\frac{u_2' p'}{\rho}\right)}$ by integrating the difference between the so-called "transport dissipation" and the "homogeneous dissipation". In this study, the pressure diffusion term will be inferred from the forced balance of the turbulent kinetic energy equation. This result will subsequently be compared with the DNS strained wake results of Moser et al (1998).

3.3
Turbulence diffusion term
The turbulence diffusion term is composed of the streamwise turbulence diffusion $-\frac{\partial}{\partial x_1}\frac{1}{2}\overline{(u_1'^3 + u_1' u_2'^2 + u_1' u_3'^2)}$ and the lateral diffusion $-\frac{\partial}{\partial x_2}\frac{1}{2}\overline{(u_1'^2 u_2' + u_2'^3 + u_2' u_3'^2)}$. In order to determine the turbulence diffusion term, an X-wire probe can be used to obtain $\overline{u_1'^3}$, $\overline{u_1' u_2'^2}$, $\overline{u_1' u_3'^2}$, $\overline{u_1'^2 u_2'}$ and $\overline{u_2'^3}$ by direct measurement. The remaining term $\overline{u_2' u_3'^2}$ can be obtained indirectly from additional X-wire measurements through application of a procedure developed by Townsend (1949) and described by Wygnanski and Fiedler (1969). Alternately, both Panchapakesan and Lumley (1993) and Hussein et al (1994) simply assumed that $\overline{u_2' u_3'^2} \approx \overline{u_2'^3}$ for their jet flow measurements, and demonstrated that the error introduced by this assumption is less than 10%. In this study, we will also use this approximation to estimate the required term $\overline{u_2' u_3'^2}$.

3.4
Turbulence production term
The shear production $-\overline{u_1' u_2'}\left(\frac{\partial \bar{U}_1}{\partial x_2} + \frac{\partial \bar{U}_2}{\partial x_1}\right)$ and dilatational turbulence production $-\left(\overline{u_1'^2} - \overline{u_2'^2}\right)\frac{\partial \bar{U}_1}{\partial x_1}$ can be measured directly. Independent measurements of turbulence production using both X-wire probes and two-component laser Doppler velocimetry (LDV) are presented in Liu et al (2002). Excellent agreement between the hot-wire and LDV measurements was obtained. These experiments show that, despite the streamwise pressure gradients imposed, the wake is shear dominated since $-\left(\overline{u_1'^2} - \overline{u_2'^2}\right)\frac{\partial \bar{U}_1}{\partial x_1} \ll -\overline{u_1' u_2'}\left(\frac{\partial \bar{U}_1}{\partial x_1} + \frac{\partial \bar{U}_2}{\partial x_1}\right)$. Despite this, we include the dilatational production term in the TKE budget. As indicated, the measurement of local turbulence production requires cross-stream profiles of both local mean velocity and Reynolds shear and normal stresses.

3.5
Viscous diffusion terms
All previously cited investigations of the turbulent kinetic energy budget in free shear flows have ignored the viscous diffusion terms. Wygnanski and Fiedler (1969) and Gutmark and Wygnanski (1976) note that neglect of these terms was based on the assertion of Laufer (1954) that the term is comparatively small in the turbulent kinetic energy equation. Panchapakesan and Lumley (1993) explained that in free turbulent flows, away from walls, the viscous contribution to the transport terms is negligible in comparison with the turbulent contribution. In the wake under investigation here, this is substantiated by the direct measurements of the local turbulent viscosity, as defined by the value of $\nu_t \equiv -\overline{u_1' u_2'}/(\partial \bar{U}_1/\partial x_2)$. Results indicate that $\nu_t/\nu \sim O(10^3)$. Neglect of the viscous diffusion term is further validated from measured values of the second derivative of the turbulence kinetic energy $\frac{\partial^2 k}{\partial x^2}$ which is $O(1.0\ s^{-2})$. This leads to a corresponding value for the viscous diffusion $O(10^{-5}\ m^2/s^3)$, which is only about 10^{-7} times the peak value of the measured viscous dissipation term. It may be noticed that by neglecting the viscous diffusion term, the only difference between Eq. 1and Eq. 2 is the expression for the dissipation term.

3.6
Dissipation term
A review of the cited literature reveals that the dissipation term can be estimated in one of five ways. In this study, three of these approaches will be utilized to obtain preliminary dissipation estimates, and the results are compared. Each of the approaches is briefly described below. Ultimately, however, we will utilize a locally axisymmetric turbulence assumption for the dissipation estimate used in the wake TKE budget.

3.6.1
Isotropic turbulence assumption
In high Reynolds number flows, the viscous dissipation takes place at the smallest scales of motion. Due to the assumed loss of directional information during the energy cascade to small scales, the turbulence may be approximated as locally isotropic, in which case the dissipation term can be radically simplified to (see Hinze 1975)

$$\varepsilon = 15\nu\overline{\left(\frac{\partial u_1'}{\partial x_1}\right)^2} \tag{4}$$

The required fluctuating spatial derivative can be obtained from the temporal derivative of u'_1 by invoking Taylor's frozen field approximation,

$$\frac{\partial}{\partial x} \approx -\frac{1}{\overline{U_1}}\frac{\partial}{\partial t} \tag{5}$$

This was the technique employed by Gutmark and Wygnanski (1976) and Bradbury (1965) for their jet flow measurements.

3.6.2
Locally axisymmetric homogeneous turbulence assumption
Using measurements in a round jet, and those of Browne et al (1987) in a cylinder wake, George and Hussein (1991) demonstrated that the mean-square derivatives of the fluctuating velocity are in good agreement with local axisymmetric turbulence theory, the characteristic feature of which is the invariance of statistical quantities with respect to rotation about a preferred direction. With the assumption of locally axisymmetric, homogeneous turbulence, the dissipation term can be estimated from either

$$\varepsilon = \nu\left[\frac{5}{3}\overline{\left(\frac{\partial u_1'}{\partial x_1}\right)^2} + 2\overline{\left(\frac{\partial u_1'}{\partial x_3}\right)^2} + 2\overline{\left(\frac{\partial u_2'}{\partial x_1}\right)^2} + \frac{8}{3}\overline{\left(\frac{\partial u_2'}{\partial x_3}\right)^2}\right] \tag{6}$$

or

$$\varepsilon = \nu\left[-\overline{\left(\frac{\partial u_1'}{\partial x_1}\right)^2} + 2\overline{\left(\frac{\partial u_1'}{\partial x_2}\right)^2} + 2\overline{\left(\frac{\partial u_2'}{\partial x_1}\right)^2} + 8\overline{\left(\frac{\partial u_2'}{\partial x_2}\right)^2}\right] \tag{7}$$

In Eq. 6, the terms $\overline{\left(\frac{\partial u'_1}{\partial x_1}\right)^2}$ and $\overline{\left(\frac{\partial u'_1}{\partial x_3}\right)^2}$ can be obtained from a temporal derivative of the $u'_1$and u'_2time-series (obtained via the X-wire), respectively, combined with the use of Taylor's frozen field approximation. The term $\left(\frac{\partial u^1_1}{\partial x_3}\right)^2$ can be obtained from a dual sensor, parallel probe measurement. The estimate of the $\left(\frac{\partial u'_2}{\partial x_3}\right)^2$ term requires a twin X-wire probe configuration, which was shown in Sect. 2.5.

3.6.3
Semi-isotropic turbulence assumption

In this approach, unmeasured fluctuating velocity derivatives in the homogeneous dissipation term are estimated based on measured fluctuating velocity derivatives. For example, the streamwise derivatives $\overline{\left(\frac{\partial u'_1}{\partial x_1}\right)^2}$, $\overline{\left(\frac{\partial u'_2}{\partial x_1}\right)^2}$, and $\left(\frac{\partial u'_3}{\partial x_1}\right)^2$ can each be estimated from temporal derivatives by invoking Taylor's hypothesis as described above. The lateral and spanwise derivatives, $\left(\frac{\partial u'_1}{\partial x_2}\right)^2$ and $\left(\frac{\partial u'_1}{\partial x_3}\right)^2$ can be obtained by closely spaced parallel hot-wire probes separated in either the $x_2$or x_3 directions. The four remaining derivatives $\overline{\left(\frac{\partial u'_2}{\partial x_2}\right)^2}$, $\overline{\left(\frac{\partial u'_2}{\partial x_3}\right)^2}$, $\overline{\left(\frac{\partial u'_3}{\partial x_2}\right)^2}$ and $\overline{\left(\frac{\partial u'_3}{\partial x_3}\right)^2}$ in thedissipation term can be subsequently estimated by invoking a semi-isotropy assumption, as described in detail by Wygnanski and Fiedler (1969), which assumes the nine spatial derivatives in the dissipation term observe the following semi-isotropy relationship:

$$\begin{aligned}
k_s\overline{\left(\frac{\partial u'_1}{\partial x_1}\right)^2} &= \overline{\left(\frac{\partial u'_2}{\partial x_1}\right)^2} = \overline{\left(\frac{\partial u'_3}{\partial x_1}\right)^2}\\
\overline{\left(\frac{\partial u'_1}{\partial x_2}\right)^2} &= k_s\overline{\left(\frac{\partial u'_2}{\partial x_2}\right)^2} = \overline{\left(\frac{\partial u'_3}{\partial x_2}\right)^2}\\
\overline{\left(\frac{\partial u'_1}{\partial x_3}\right)^2} &= \overline{\left(\frac{\partial u'_2}{\partial x_3}\right)^2} = k_s\overline{\left(\frac{\partial u'_3}{\partial x_3}\right)^2}
\end{aligned} \tag{8}$$

where k_s is the semi-isotropy coefficient. In the present study, the coefficient k_s will be determined from the streamwise mean square derivative measurements.

3.6.4
Direct measurement of all nine fluctuating derivative terms

Of course, the most sophisticated method for obtaining the dissipation is to measure all nine fluctuating derivative terms by use of twin X-wires, as described by Browne et al (1987). Their bluff body wake study indicated that the local isotropy assumption is not valid for a cylinder wake in the self-preserving region with relatively low Reynolds number. However, the requirement of twin X-wires severely limits the spatial resolution of the fluctuating derivative measurements. In the present study we will not use this approach since the spatial resolution of the twin X-wire probe configuration was deemed too large to obtain a reliable measurement of the required derivatives.

3.6.5
Forced balance of the TKE equation

The easiest way to evaluate the dissipation term is from a forced balance of the turbulent kinetic energy equation. However, this approach assumes that the pressure transport term is negligible, which we will subsequently demonstrate is not the case. Therefore, this approach will not be used in this study.

3.7
Measurement of streamwise derivatives of mean quantities

For the finite-difference approximation of streamwise derivatives of *mean quantities*, the selection of the distance Δx between adjacent streamwise stations will greatly affect the measurement uncertainty. In the measurements reported here, Δx was optimized using an uncertainty analysis. With profiles of a given mean turbulence quantity obtained at three consecutive streamwise measurement stations, a natural approach for taking the spatial derivative of a given function $f(x)$ would be to use a central-difference approximation with x_i=x, (x_i–x_{i-1})=Δx and (x_{i+1}–x_i)=Δx. This gives,

$$\frac{df}{dx} = \frac{f_{i+1} - f_{i-1}}{2\Delta x} + O\left((\Delta x)^2\right) \tag{9}$$

It may be shown (Gerald and Wheatley 1994) that the numerical differentiation based on evenly-spaced quadratic Lagrangian polynomial interpolation is identical to the central difference scheme. If there is no positioning error associated with the probes, the uncertainty of the estimate of $\frac{df}{dx}$ is solely determined by truncation, which is basically a bias error due to the use of the central-difference scheme. This will obviously decrease as Δx decreases, which would suggest that we want the spacing between the adjacent measurement stations to be as close as possible. However, in reality, there are unavoidable positioning errors associated with both the streamwise and lateral locations of the probe. With this positioning error, the behavior of the uncertainty of $\frac{df}{dx}$ will be totally different. Assuming δx and δy positioning errors associated with the x and y locations of the probe, respectively, the propagation of these errors to the finite difference representation of $\frac{df}{dx}$ was investigated. This reveals that uncertainty in $\frac{df}{dx}$ due to probe positioning uncertainty actually *increases* as Δx decreases. Therefore, the total uncertainty in $\frac{df}{dx}$ is comprised of two parts, that due to positioning error, which decreases with Δx, and that due to truncation error, which increases with Δx. This aspect is clearly shown in Fig. 3, which compares the variation of position, truncation and total uncertainties of dk/dx with Δx. Note that the two competing trends give rise to an optimal Δx separation for the measurements. In this study, the TKE budget measurements were obtained at the streamwise location x=101.6 cm (x/θ_0=141) for the ZPG, APG, and FPG cases. Based on an uncertainty analysis like that described above, the optimal streamwise separation of the measurement stations was selected as Δx=12.7 cm. Therefore multiple traverses at streamwise locations x_{i-1}=88.9 cm, x_i= 101.6 cm and x_{i+1}=114.3 cm were obtained as described in Liu (2001).

4
Results for the zero pressure gradient wake

In this section we separately present each of the measured terms in Eq. 3 for the ZPG turbulent wake case. These

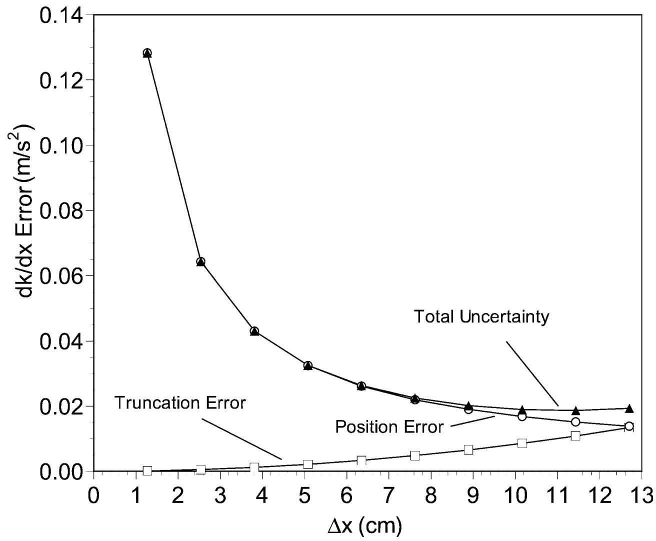

Fig. 3. Uncertainty analysis of dk/dx for ZPG at x=101.6 cm, y=0.0 cm

results were obtained by the methods outlined in the previous section.

4.1 Convection term

The lateral distribution of the streamwise convection $-\bar{U}_1\frac{\partial k}{\partial x_1}$, the lateral convection $-\bar{U}_2\frac{\partial k}{\partial x_2}$, and their sum for the symmetric wake in ZPG at x/θ_0=141 are presented in Fig. 4. In this figure, both convection terms are non-dimensionalized by using the local wake half-width δ(x) as the reference length scale, and the local maximum velocity defect U_d(y) as the reference velocity scale. Here δ is defined as the lateral distance from the centerline of the wake to the position at which the local velocity defect drops to half of U_d. From Fig. 4, it can be seen that for the symmetric wake in ZPG, the streamwise convection dominates the total convection distribution.

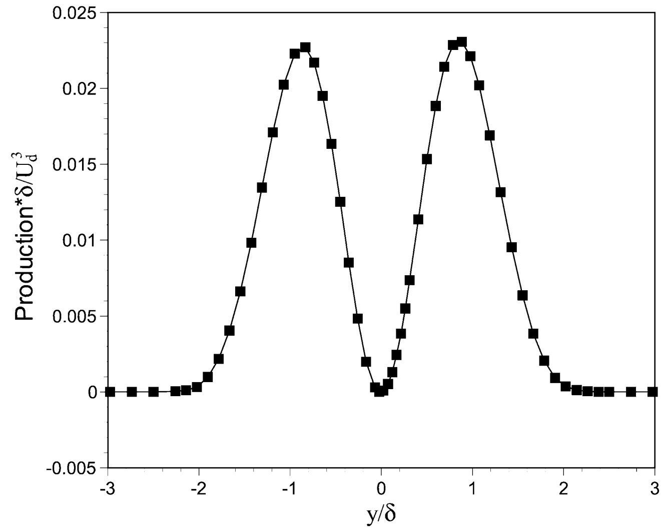

Fig. 5. Turbulent production in the ZPG symmetric wake at x/θ_0=141

4.2 Production term

For the ZPG wake, the dilatational production $-\left(\overline{u_1'^2}-\overline{u_2'^2}\right)\frac{\partial \bar{U}_1}{\partial x_1}$ is zero. Figure 5 presents the measured shear production term (simplified as $-\overline{u_1'u_2'}\frac{\partial \bar{U}_1}{\partial x_2}$ since $\frac{\partial \bar{U}_2}{\partial x_1}\approx 0$) as obtained for the ZPG wake at x/θ_0=141. The production has been appropriately scaled by local values of $\delta(x)$ and $U_d(x)$. Peak turbulence production is symmetric across the wake, and occurs near y/δ=±0.9, which is associated with the lateral location of maximum mean strain rate $\frac{\partial \bar{U}_1}{\partial x_2}$. Very similar results were obtained from a separate flow field survey of the symmetric wake using LDV, as presented in Liu et al (2002).

4.3 Turbulence diffusion term

Figure 6 presents measured profiles of the streamwise turbulence diffusion $-\frac{\partial}{\partial x_1}\frac{1}{2}\overline{(u_1'^3+u_1'u_1'^2+u_1'u_3'^2)}$and the

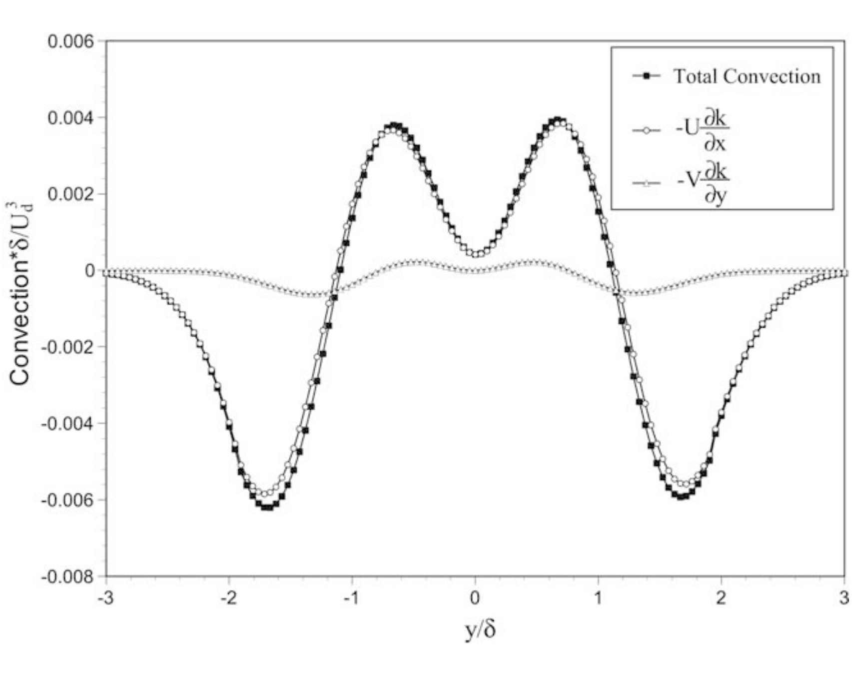

Fig. 4. Convection in the ZPG symmetric wake at x/θ_0=141

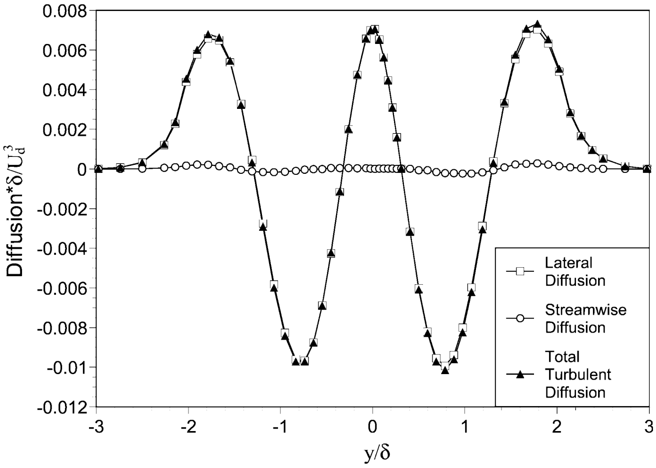

Fig. 6. Turbulence diffusion in the ZPG symmetric wake at x/θ_0=141

lateral turbulence diffusion $-\frac{\partial}{\partial x_2}\frac{1}{2}\overline{(u_1'^2u_2' + u_2'^3 + u_2'u_3'^2)}$for the symmetric wake in ZPG at x/θ_0=141. The diffusion terms have been scaled appropriately by local values of δ and U_d. It is apparent from this figure that for the ZPG turbulent wake, the lateral turbulent diffusion is the dominant diffusion mechanism. By comparison, the streamwise turbulence diffusion is negligible. Since streamwise turbulence diffusion is not significant and the lateral diffusion serves only to locally redistribute turbulence kinetic energy, we expect that cross-stream integration should give,

$$\int_{-\infty}^{+\infty}\left[-\frac{\partial}{\partial x_2}\frac{1}{2}\overline{(u_1'^2u_2' + u_2'^3 + u_2'u_3'^2)}\right]dx_2 = 0$$

In order to gauge the accuracy of the measurement of the lateral diffusion term, the profile of the total turbulence diffusion shown in Fig. 6 was numerically integrated across the wake, and the result was indeed found to be zero (within experimental uncertainty).

4.4 Dissipation term

Among all of the terms in the turbulence kinetic energy equation, the measured dissipation term is most likely to possess significant bias error. There are two primary error sources associated with the dissipation estimate. First, as described in Sect. 3, since we neglect the cross-derivative correlation terms and resort to the homogeneous approximation for dissipation, this will give rise to a bias error due to mathematical modeling. Second, the limited spatial resolution of the hot wire probes required for the mean-square derivative measurements will give rise to a bias error due to spatial resolution.

For the mean-square derivatives there are two requirements for a reliable measurement. First, the spatial resolution of the probe should resolve scales on the order of the Kolmogorov length scale; second, the temporal resolution of the velocity fluctuation time-series record should capture the highest frequencies associated with the convection of dissipative scales past the sensor(s). There is little difficulty in fulfilling the temporal resolution requirement based on the available probe size. Therefore, the Nyquist frequency of the data record provides a sufficient match to the temporal resolution requirement.

Regarding the spatial resolution requirement, unfortunately, as described in Sect. 2.5, the dimensions of the hot-wire sensors and their spacing in multi-sensor configurations are all greater than the Kolmogorov length scale, which is approximately 0.1 mm near the centerline of the wake. However, probe spatial resolution is critical for a reliable mean-square derivative estimate, as described in detail by Wallace and Foss (1995). Through an investigation of the effect of the finite-difference spacing on the mean-square derivative estimate obtained from DNS data, Wallace and Foss demonstrated that the estimate of the mean-square derivative is attenuated dramatically as finite difference spacing is increased, which is equivalent to the issue of probe spatial resolution in the measurement.

The effect of spatial resolution on fluctuating derivative estimates can be clearly seen by comparing the same fluctuating derivative as measured by the dual sensor parallel probe with that from the X-wire. Consider, for example, the mean square derivative term $\overline{\left(\frac{\partial u_1'}{\partial x_1}\right)^2}$, which can be obtained from measured time-series data by invoking Taylor's frozen field hypothesis. All results obtained for $\overline{\left(\frac{\partial u_1'}{\partial x_1}\right)^2}$ using both X-wire and parallel probes under ZPG conditions are shown in Fig. 7. From this figure, it can be seen that although the cross-stream profile shapes are the same, the parallel probe gives higher peak values for the quantity $\overline{\left(\frac{\partial u_1'}{\partial x_1}\right)^2}$ than the X-wire probe does. This disparity can be attributed to the difference between the effective measurement volume of the parallel and X-wire probes. In particular, Fig. 7 clearly illustrates that the larger effective measurement volume of the X-wire results in a lower mean-square derivative measurement due to effective spatial low-pass filtering. Therefore $\overline{\left(\frac{\partial u_1'}{\partial x_1}\right)^2}$, as measured by the parallel probe will be closer to the true value than the corresponding X-wire measurement, although it too will be biased by some degree due to insufficient spatial resolution.

In this study, the bias error associated with the dissipation measurement was minimized via a two-step procedure. First, for those fluctuating derivatives that can be measured by both the parallel probe and X-wire (or X-wire pair), the degree by which the magnitude of the fluctuating derivative is reduced (relative to the parallel probe) due to probe spatial resolution limitations was quantified. In each of these comparisons, the cross-stream profiles of fluctuating derivatives had identical shapes but the magnitudes were reduced below those measured by the parallel probe configuration. This allowed the determination of correction factors to be applied to those fluctuating derivatives that could only be measured by the X-wire (or X-wire probe pair). This *partially* compensated the magnitude of the fluctuating derivative to an equivalent effective resolution of the parallel probe. The only assumption required is that the scaling factor would be the same for those derivatives in which we have no corresponding parallel

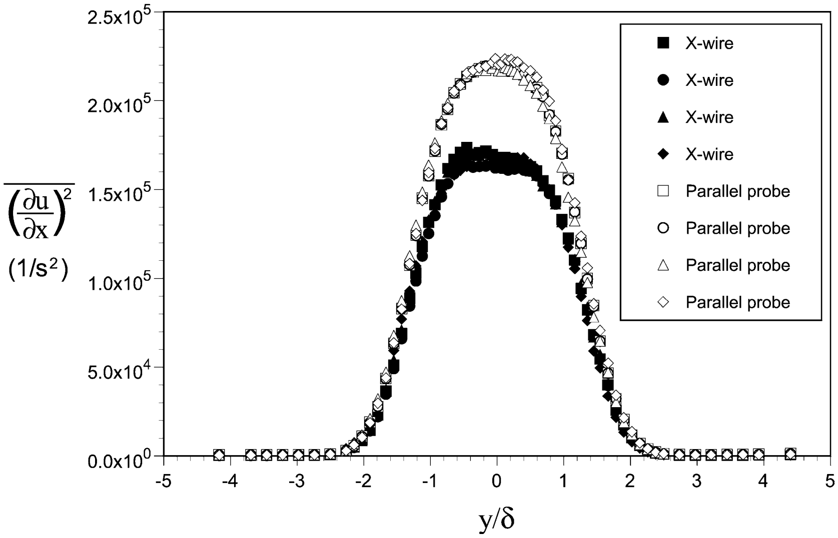

Fig. 7. Comparison of $\overline{\left(\frac{\partial u_1'}{\partial x_1}\right)^2}$ measured by X-wire and parallel probes in the ZPG symmetric wake at x/θ_0=141

probe measurement. Once the derivatives were partially compensated in this manner, preliminary estimates of the dissipation term were made by making the local isotropy, locally axisymmetric turbulence, and quasi-isotropic turbulence approximations, as outlined in Sect. 3.6. These preliminary dissipation estimates are compared in Fig. 8, where it can be seen that significant disparities occur between estimates. Note that the dissipation term based on the local isotropy assumption is much smaller in magnitude than for the other two methods.

Each of the preliminary dissipation estimates was incorporated into the wake TKE budget Eq. 3 (along with the other measured terms) and the pressure diffusion term was extracted from a forced balance. Since the pressure diffusion term serves primarily to locally redistribute turbulent kinetic energy, one expects that a cross-stream integration of this term should be very close to zero (as was previously demonstrated for the measured turbulence diffusion). In fact, the accuracy of each preliminary dissipation estimate was assessed by checking the lateral integration character of the resulting pressure diffusion term in each case. It was found that the dissipation estimate based on the locally axisymmetric turbulence assumption leads to a result in which cross-stream integration of the pressure diffusion is closest to zero. The idea of using the zero cross-stream integration character of turbulence diffusion to assess the accuracy of dissipation is not unique to our study. In his measurement of the TKE budget of a turbulent planar jet, Bradbury (1965) assumed local isotropy in his measurement of dissipation, and this was subsequently corrected by requiring that the sum of the pressure and turbulence diffusion terms (extracted from a forced balance) should exhibit zero integration across the jet.

In the current study, the pressure diffusion term obtained from the forced balance of the TKE equation includes not only the pressure diffusion itself, but also an error term. The error term can be further decomposed into bias and random error components. The random error component would not be expected to exhibit a systematic variation across the wake, and consequently its effect is likely to be canceled upon cross-wake integration.

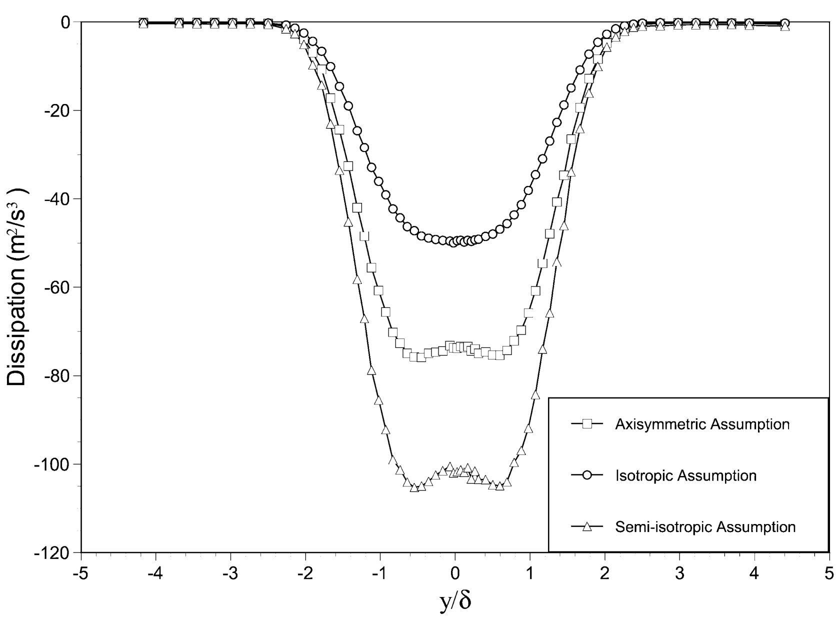

Fig. 8. Comparison of dissipation estimates for the ZPG symmetric wake at x/θ_0=141

However, the bias error will clearly remain. If we make the plausible assumption that the dissipation, including both the measured mean-square derivative terms and the unmeasured cross-derivative correlation terms, is the dominant source of this bias error, then reducing the bias error associated with the dissipation should bring the cross-wake integration of the pressure diffusion term to zero.

The attribute of zero lateral integration of the pressure diffusion term can be utilized as a constraint to correct the bias error associated with the axisymmetric turbulence dissipation estimate. More specifically, with the pressure diffusion term obtained from the forced balance of the TKE equation, we can use a shooting method to iteratively adjust a constant scaling factor to be applied to the dissipation term until we get a zero lateral integration of the pressure diffusion. The constant scaling factor serves to compensate the bias error due to insufficient spatial resolution of measurement probes, as well as the bias error due to the mathematical modeling of the dissipation term.

4.5
ZPG turbulent kinetic energy budget

Figure 9 presents cross-stream profiles of the terms in Eq. 3 for the ZPG planar wake at x/θ_0=141. The viscous diffusion term is assumed to be negligible. All terms except pressure diffusion have been obtained from direct measurement. Error bars associated with the measured terms are also shown in this figure. Note that these error bars reflect only the uncertainty associated with measurement and data analysis. The uncertainty in the dissipation associated with mathematical modeling is not included. The pressure diffusion profile shown in Fig. 9 is obtained by forcing a balance of the TKE equation, and therefore it actually consists of both the true pressure diffusion and the (minimized) total error of the measurement. All terms in Fig. 9 have been scaled in a consistent manner with local values of $\delta$and U_d. Positive values indicate a local gain in TKE while negative values indicate a loss. Note for example, that turbulence dissipation is always negative and production positive. This figure presents the turbulence dissipation corrected such that cross-wake integration of the pressure diffusion term is zero.

The double peaks of the production term correspond approximately to the locations of the maximum mean strain rate in the upper and lower shear layers of the wake. At the center or near the edges of the wake, the mean shear is zero or asymptotically approaches zero, and there is no production.

Note that both turbulence diffusion and pressure diffusion terms have similar profile shapes. The diffusion terms respond to the lateral gradient in turbulent kinetic energy associated with newly-generated turbulence resulting from the production term. Both terms clearly serve to transport turbulence laterally away from regions of high mean strain, where it is produced, and toward those locations with low production (like the wake centerline and outer edges). Note also that while turbulence diffusion is greater than pressure diffusion, the latter term is certainly not negligible as has often been assumed. In addition, there is no evidence in Fig. 9 that there is a so-called counter-gradient transport mechanism for the pressure diffusion term, as suggested by Demuren et al (1996).

As for the dissipation term, it can be seen from Fig. 9 that the greatest dissipation occurs across the central region of the wake, where the turbulence level is most intense.

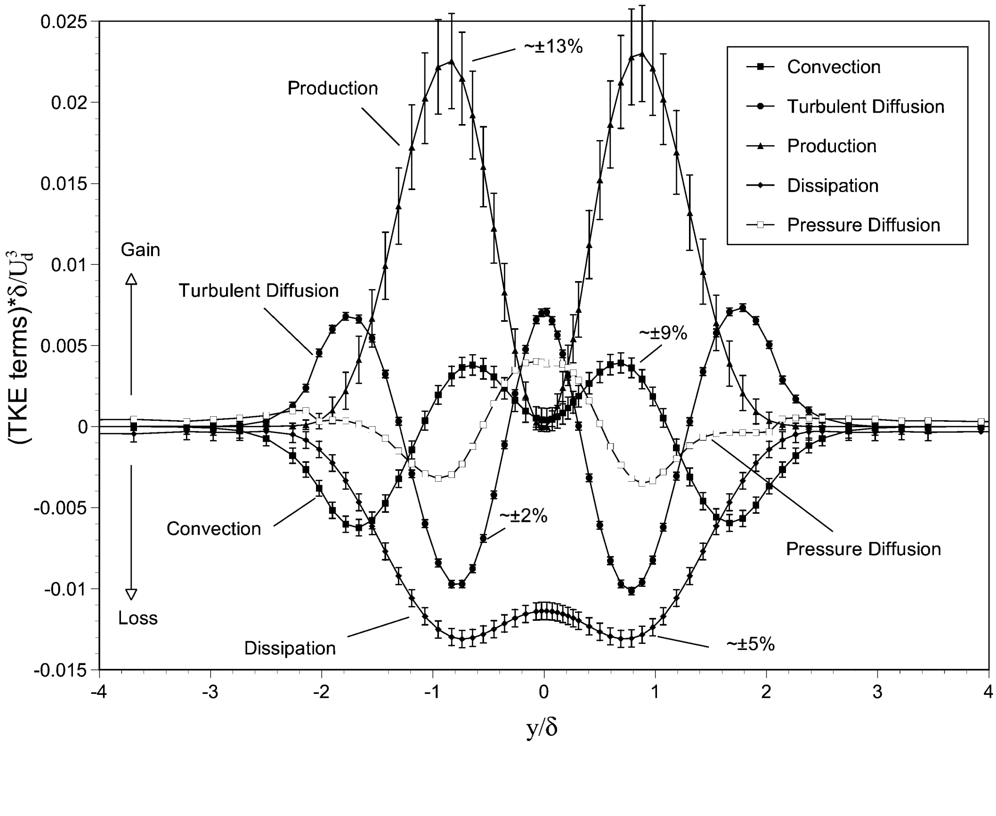

Fig. 9. Turbulent kinetic energy budget for the planar wake in ZPG at x/θ_0=141

4.6
Comparison with DNS results

Moser et al (1998) investigated the TKE budget of a temporally evolving planar turbulent wake using DNS. They applied forcing to the initial wake, and then investigated the influence of the forcing on the far wake development. Their unforced wake corresponds to the ZPG conditions of our wake study, with three basic differences: (1) they obtained the TKE budget in the far wake similarity region while ours is obtained in the near-wake region; (2) their wake develops in the temporal domain while ours obviously develops spatially; and, (3) their mass-flux Reynolds number, which is equivalent to the momentum-thickness Reynolds number in spatially developing wakes, is only 2000, an order of magnitude smaller than ours (Re_θ=15000).

For the temporally-developing wake flow in DNS, the only non-zero mean velocity component is $\bar{U}_1$, and due to homogeneity in the streamwise and spanwise directions, derivatives of averaged quantities with respect to x_1 and x_3 are zero. For the experiment, the spatially-developing wake flow is homogeneous in time t and spanwise direction x_3. Therefore, in the Reynolds stress transport equation labeled as A1 in Moser et al (1998), there is no streamwise or lateral convection term for the Reynolds stress transport. However, the temporal derivative term in DNS can be transformed into the streamwise convective term in the spatial domain, and vice versa, through the following relationship:

$$\frac{\partial}{\partial t} = U_e \frac{\partial}{\partial x} \qquad (10)$$

where U_e is the external free stream velocity outside of the wake in the spatial domain. Figure 12a in Moser et al (1998) provides the budget of the quantity of $\overline{q^2}(= 2k)$ for the temporally-developing wake simulated by DNS. By using the transformation specified by (10), we can make direct comparisons of our experimental data with the DNS results. The time derivative term in DNS matches the streamwise convection term in the experiment, and production, turbulence diffusion, pressure diffusion, and dissipation in DNS match the corresponding terms in the experiment. The only term left unmatched is the lateral convection term in the experiment. More specifically, in order to make a fair comparison with the DNS results, the experimentally-measured terms in Eq. 3 need to be scaled by $\frac{U_d^3}{4\delta}\left(\frac{U_1}{U_e}\right)$. In this manner, the streamwise convection term in the experiment will have the same scale as the time derivative of $\overline{q^2}$shown in Fig. 12a of Moser et al (1998).

Figures 10, 11, 12, 13, and 14 present comparisons between the experimental and DNS profiles of the dissipation, production, streamwise convection, turbulence diffusion, and the pressure diffusion, respectively. In these figures, open circles represent the experimental results and the solid line represents the DNS simulation. Considering the different Reynolds numbers and stages of wake development for the experiments and simulations, the agreement between the experimental and DNS results is quite encouraging. In particular, the agreement between the measured and DNS-based turbulent diffusion term is quite remarkable. Even the comparison of the pressure diffusion terms shows good general agreement. Note that the scatter of the DNS data for the pressure diffusion term

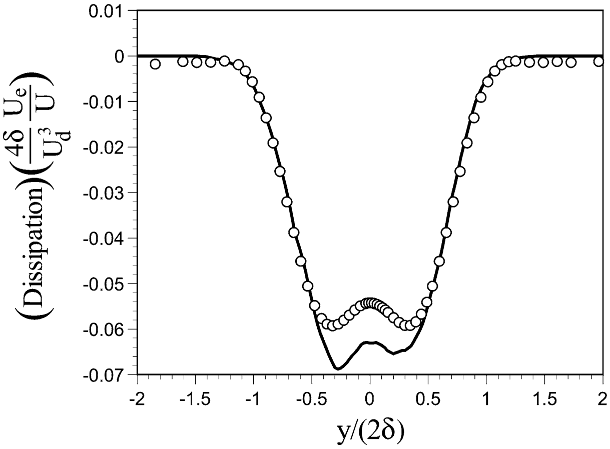

Fig. 10. Comparison of experimental and DNS (Moser et al 1998) dissipation profiles for the symmetric wake in ZPG

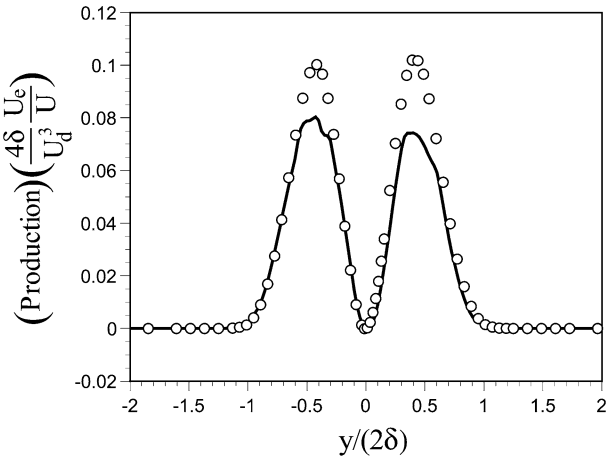

Fig. 11. Comparison of experimental and DNS (Moser et al 1998) production profiles for the symmetric wake in ZPG

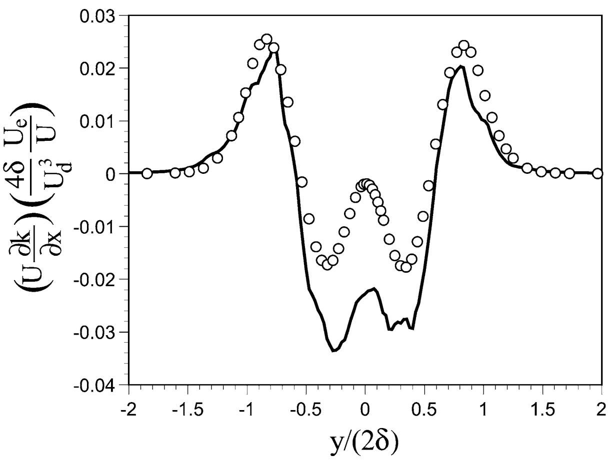

Fig. 12. Comparison of experimental and DNS (Moser et al 1998) convection profiles for the symmetric wake in ZPG

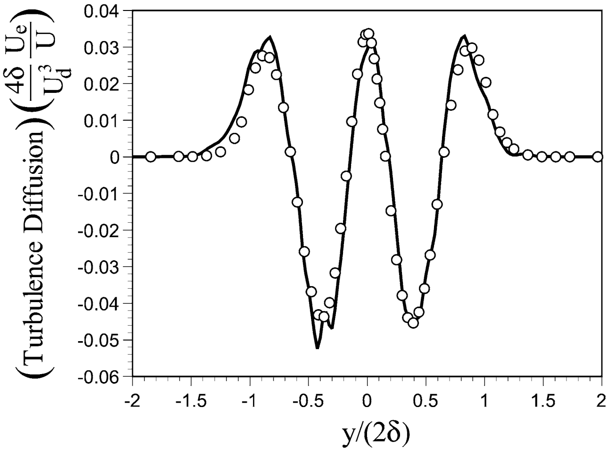

Fig. 13. Comparison of experimental and DNS (Moser et al 1998) turbulence diffusion profiles for the symmetric wake in ZPG

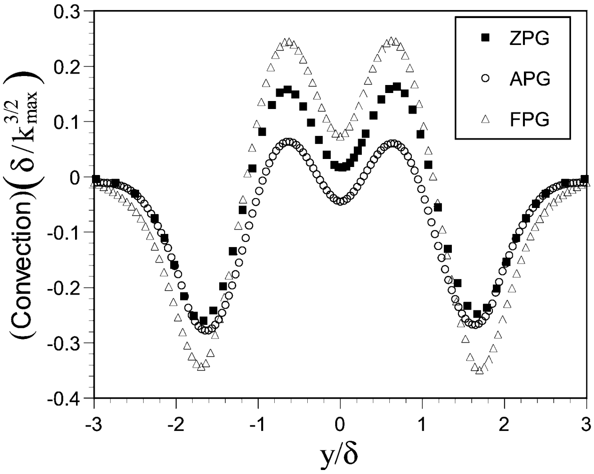

Fig. 15. Comparison of the convection profiles for the symmetric wake in ZPG, APG and FPG

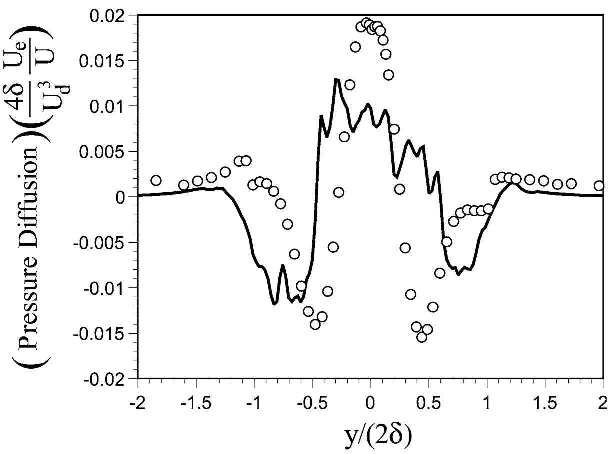

Fig. 14. Comparison of experimental and DNS (Moser et al 1998) pressure diffusion profiles for the symmetric wake in ZPG

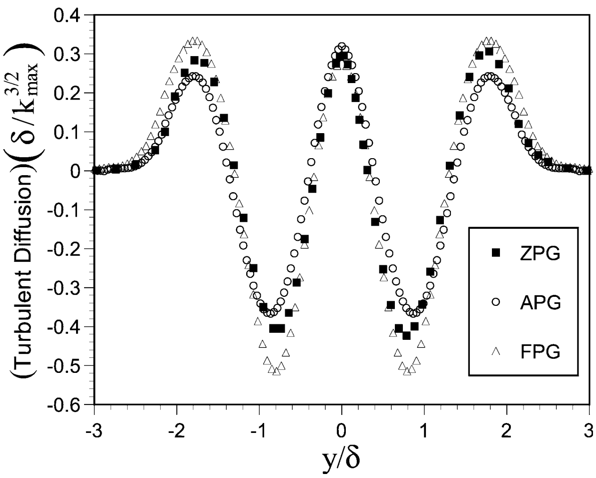

Fig. 16. Comparison of the turbulence diffusion profiles for the symmetric wake in ZPG, APG and FPG

is likely due to an insufficient period for the time-averaging. Note also that the experimental pressure diffusion term contains not only the pressure diffusion itself, but also the total measurement error of the TKE budget. Therefore, the comparison of the pressure diffusion terms can also be viewed as a measure indicating the overall accuracy and reliability of the TKE budget measurement. Observed disparities between the convection, production and dissipation terms can be attributed to different Reynolds numbers and different stages of development between the experimental and the DNS data. Moreover, the disparity between the convection terms of the experimental and DNS data may also be attributed largely to the absence of lateral convection for the DNS simulation, which evolves temporally as a strictly parallel flow.

5 Effect of the pressure gradient on the planar wake TKE budget

To investigate the influence of the pressure gradient on the wake TKE budget, terms for the ZPG, APG, and FPG cases were normalized by using the local wake half-width δ, and the square root of the local maximum turbulent kinetic energy $\sqrt{k_{max}}$, as the reference length and velocity scales, respectively. The comparisons between the normalized TKE budget terms for different pressure gradient cases are presented in Figs. 15, 16, 17, and 18.

As reported in Liu et al (2002), when the adverse pressure gradient is imposed, the wake widening rate is enhanced, the velocity defect decay rate is reduced, and the turbulence intensity and the Reynolds stress are both amplified. In contrast, when the wake develops in a favorable pressure gradient, the wake widening rate is reduced, the velocity defect decay rate is increased, and the turbulence intensity and Reynolds stress are both decreased in relation to corresponding zero pressure gradient values. The wakes studied in this paper are all shear-dominated, despite the imposed streamwise straining. However, as noted in Liu et al (2002), the dilatational production term is found to play an important role in augmenting and suppressing the turbulence for the APG and FPG cases, respectively. Acting as a trigger, this term

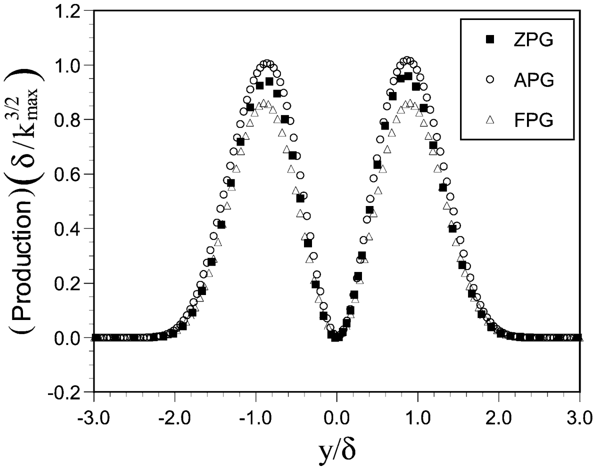

Fig. 17. Comparison of the turbulence production profiles for the symmetric wake in ZPG, APG and FPG

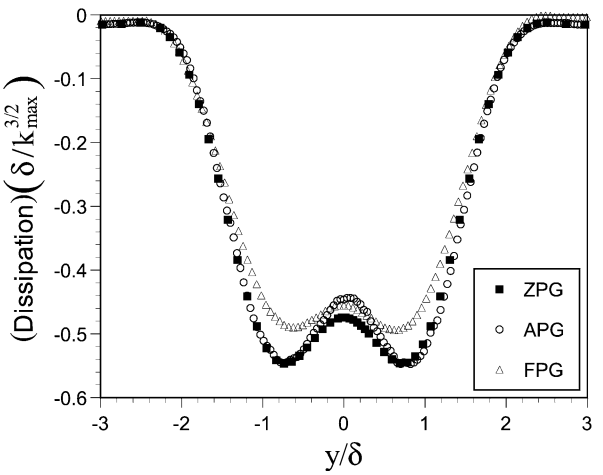

Fig. 18. Comparison of the dissipation profiles for the symmetric wake in ZPG, APG and FPG

gives rise to an initial disparity in turbulence levels after imposition of the pressure gradients, and subsequently alters the shear production term through modification of $-\overline{u'v'}$. Measurements of the Reynolds stress correlation suggest no significant modification in the phase relationship between u' and v' due to the imposed pressure gradients. Cross-stream profiles of $-\overline{u'v'}/k$ obtained at various streamwise locations exhibit collapse for each pressure gradient case investigated.

Consistent with this scenario, Fig. 17 clearly shows local turbulence production for the APG case exceeds that for ZPG. In contrast, production for the FPG case is suppressed below that for ZPG. These differences are directly associated with the dilatational production term. The effect of the imposed pressure gradient is also significant for the convection term, as shown in Fig. 15, since this term is directly related to the mean motion of the flow field. As expected, streamwise convection is greatest for the accelerated FPG case and less so for the APG. Given the effect that the pressure gradient has on the turbulence production term (as shown in Fig. 17), it is not surprising that the turbulence diffusion exhibits comparable disparities among the imposed pressure gradient cases, as shown in Fig. 16. In contrast, Fig. 18 indicates that the influence of pressure gradient on dissipation is minimal compared to the other terms. *These comparisons suggest that the fundamental TKE transport mechanism is not altered by the imposed pressure gradients*. Rather, Figs. 15, 16, 17, and 18 suggest that the imposed pressure gradient exerts its influence on the turbulence field primarily through the mean flow and largest scale energy-containing motions rather than the fine-scale turbulence.

6
Conclusions

A series of turbulent kinetic energy (TKE) budget measurements were conducted for a symmetric, turbulent planar wake flow subjected to constant zero, favorable, and adverse pressure gradients. Special consideration was given to the dissipation estimate. On the basis of experimental evidence supporting similar profile shapes for the measured mean-square derivatives, and requiring zero cross-stream integration of the pressure diffusion term (obtained from the forced balance of the TKE equation), a dissipation bias error correction method was proposed and implemented in the experiments. More specifically, a scaling factor was determined using a shooting method, and applied to the dissipation estimate to compensate the bias errors due to the limited spatial probe resolution and modeling of the dissipation term. This approach is validated through the comparison of the experimental TKE budget with the DNS results obtained by Moser et al (1998). Although the stage of wake development and Reynolds numbers are different for the experiments and DNS simulations, good general agreement is observed.

Comparison of the different terms in the TKE budgets of the wake subjected to the imposed adverse, zero, and favorable pressure gradients indicates that the fundamental TKE transport mechanism is not altered by the imposed pressure gradients. The imposed pressure gradient exerts its influence on the turbulence field primarily through the mean flow and largest scale energy-containing motions rather than the fine-scale dissipative turbulence.

References

Bradbury LJS (1965) The structure of a self-preserving turbulent plane jet. J Fluid Mech 23(1):31–64

Browne LW, Antonia RA, Shah DA (1987) Turbulent energy dissipation in a wake. J Fluid Mech 179:307–326

Carlson JR, Duquesne N, Rumsey CL, Gatski TB (2001) Computation of turbulent wake flows in variable pressure gradient. Comput Fluids 30:161–187

Demuren AO, Rogers MM, Durbin P, Lele SK (1996) On modeling pressure diffusion in non-homogeneous shear flows. In: Proc Summer Program 1996, Center of Turbulent Research, Stanford University, Stanford, CA

Faure T, Robert G (1996) Turbulent kinetic energy balance in the wake of a self-propelled body. Exp Fluids 21:268–274

George WK, Hussein HJ (1991) Locally axisymmetric turbulence. J Fluid Mech 233:1–23

Gerald CF, Wheatley PO (1994) Applied numerical analysis. Addison-Wesley, Reading, MA

Gutmark E, Wygnanski I (1976) The planar turbulent jet. J Fluid Mech 73(3):465–495

Heskestad G (1965) Hot-wire measurements in a plane turbulent jet. J Applied Mech–T ASME 32:721–734
Hinze JO (1975) Turbulence. McGraw-Hill, New York.
Hussein HJ, Capp SP, George WK (1994) Velocity measurements in a high-Reynolds-number, momentum-conserving, axisymmetric, turbulent jet. J Fluid Mech 258:31–75
Laufer J (1954) The structure of turbulence in fully developed pipe flow. NACA Report 1174
Liu X (2001) A study of wake development and structure in constant pressure gradients. PhD dissertation, University of Notre Dame, Notre Dame, IN
Liu X, Thomas FO, Nelson RC (2002) An experimental investigation of the planar turbulent wake in constant pressure gradient. Phys Fluids 14(8):2817–2838

Moser RD, Rogers MM, Ewing DW (1998) Self-similarity of time-evolving plane wakes. J Fluid Mech 367:255–289
Panchapakesan NR, Lumley JL (1993) Turbulence measurements in axisymmetric jets of air and helium, Part 1: Air jet. J Fluid Mech 246:197–223
Patel VC, Sarda OP (1990) Mean-flow and turbulence measurements in the boundary layer and wake of a ship double model. Exp Fluids 8:319–335
Raffoul CN, Nejad AS, Gould RD (1995) Investigation of three-dimensional turbulent transport behind a bluff body. In: ASME Symp Separated and Complex Flows – Joint ASME/JSME Fluids Eng Conf, FED 217, Hilton Head, South Carolina, Aug 1995, ASME, pp 121–128
Townsend AA (1949) Momentum and energy diffusion in the turbulent wake of a cylinder. P Roy Soc Lon A 197:124–140
Wallace JM, Foss JF (1995) The measurement of vorticity in turbulent flows. Annu Rev Fluid Mech 27:469–514
Wygnanski I, Fiedler H (1969) Some measurements in the self-preserving jet. J Fluid Mech 38(3):577–612
Wygnanski I, Fiedler HE (1970) The two-dimensional mixing region. J Fluid Mech 41(2):327–361